# Failure load prediction of a tubular bonded structures using a coupled criterion

Jérémy Le Pavic, Thomas Bonnemains, Éric Lolive, Georgios Stamoulis, David da Silva, David Thevenet

# Failure load prediction of a tubular bonded structures using a coupled criterion

Jérémy Le Pavic[a,b,*], Thomas Bonnemains[c], Éric Lolive[c], Georgios Stamoulis[c], David Da Silva[b], David Thévenet[a]

[a] Ensta Bretagne, UMR CNRS 6027, IRDL, F-29200 Brest, France
[b] ArianeGroup, Rue du Général Niox, F-33165 Saint Médard en Jalles, France
[c] Univ. Bretagne Occidentale, UMR CNRS 6027, IRDL, F-29200 Brest, France

In the context of increasing use of adhesive bonding for mechanical assembly, there is a need for reliable design tools. Both energetic and stress based conditions are necessary to predict the strength of bonded joints, which explains the use of a coupled criterion. The application of the criteria was performed by using Finite Element Analysis. Results obtained numerically were compared to experimental data from tubular bonded samples. A modification of the coupled criterion was proposed to take into account the loading rate in the prediction of the failure load. A good agreement was obtained between experimental and numerical predictions.

## 1. Introduction

Adhesive bonding presents several assets such as weight lightening, assembly of dissimilar material and modularity.

Because of the mismatch of properties between substrate and adhesive a singular stress field occurs especially near the edge of the adhesive layer. The stress distribution in the bondline is strongly affect by these stress concentrations; this phenomenon is called edge effect. As the result a detailed analysis is required in order to assess the numerical prediction of bonded structure. In order to design bonded structure with high reliability, several strategies have been develop in the past. Previous works study this singular behavior of two dissimilar wedge regions and propose a solution presented in [1]. More recent works proposed a methodology to describe the singular stress field for structure under tension and bending with variation of bondline thickness and dissimilar substrates [2]. This methodology of estimation of the intensity of singular stress field was used to predict the failure of single lap joint [3] cylinder butt joint [4] and also double lap joint [5]. Other authors proposed design rules based on analytical models and testing of custom specimens to take into account the strong multi-axial loading at the joint [6]. Dragoni et al. present useful software to help the engineer in the everyday design of bonded joints based on this method [7]. Finite Element Analysis (FEA) is widely used to design structures. In order to cope with singular stress fields, Point Stress criterion could be performed [8,9]. Simplicity is one of the main assets of this method. However, it requires a substantial materials database and the results are closely related to the mesh size. The presented criterion were stress-based, energetic approach have been develop.Cohesive Zone Model (CZM) exhibits excellent results to determine the failure load of bonded joints. However, the computational cost of this method is high and could not be used in early stage of design. The coupled criterion [10] propose to combine both approaches to predict the failure of bonded structure. This criteria exhibit good results when applied to single lap joint [11].

In the present paper, a tubular bonded joints are designed using a Finite Element model. The aim of the present study is to estimate the failure load of a bonded structure based on adhesive data base which require ultimate stress and fracture toughness. The first section is dedicated to the explanation of the coupled criterion. Adhesive materials are sensitive to loading rate, temperature and humidity. A modification of the coupled criterion is proposed in this paper to take into account the loading rate of a bonded structure. The coupled criterion requires a smaller material database. In this paper, the commercial adhesive EA 9395 is used. Tests were performed with three different loading rates by using the modified Arcan device. Failure envelopes were built and exhibited an influence of the loading rate on the failure strength of the bonded joint. The material toughness in modes I and II were calculated by previous authors by using DCB [12] and ENF tests [13]. In this paper, the fracture toughness is presumed to be independent of the loading rate. In order to validate the failure load prediction obtained with the coupled criterion, a tubular sample composed of two co-axial substrates bonded by adhesive layers is also used in this study. This specimen exhibits a strong multi-axial

* Corresponding author at: Ensta Bretagne, UMR CNRS 6027, IRDL, F-29200 Brest, France.
*E-mail address:* jeremy.le_pavic@ensta-bretagne.org (J. Le Pavic).

stress field at the extremities of the joint due to the edge effects. A previous study [14] focused on the failure load prediction of bonded sample under bi-axial loading by performing coupled criterion methodology. In addition, complex loading (tension/torsion) could be applied on this kind of specimen [15]. However, in the present study, only tension loading will be performed. The influence of the bondline thickness and the overlap length is investigated in this paper. For one configuration, samples were tested with two loading rates in order to assess the proposed modification of the coupled criterion. The next section explains the development of a tubular bonded sample. After assessment of the tubular sample set-up, an experimental campaign was performed and compared to the numerical failure load prediction.

## 2. Materials and methods

### 2.1. Adhesive properties

In this study an epoxy based bi-component resin (Loctite Hysol EA 9395 commercialized by Henkel) was used and showed highly fragile behavior [13,12]. The resin and the crosslinking agent were mixed at a weight ratio of 100:17, as also recommended in the datasheet of the adhesive, by means of a speed-mixer machine (DAC 150.1 FV-K) in order to obtain a homogenous mixture. The adherents were made from aluminum alloy; they were cleaned prior to bonding by immersion in pure 99% acetone for 2 h and then dried in an oven at 120 °C for 1 h. The surfaces of the substrates were ground mechanically with SiC paper (grade 180) in order to prepare them for bonding. Any final residues remaining after this procedure were simply wiped off also by means of pure 99% acetone. The adhesive was applied on both substrates manually with a spatula. The assembled specimens were cured at 76 °C for 90 min.

### 2.2. Arcan device

Arcan tests were used to identify the mechanical properties of the adhesive material. The substrates used were made of 2024 aluminum alloy. The thickness of the joint ($t_a$) was set at 0.4 mm. In order to guarantee proper alignment and good repeatability of the thickness at a tolerance of ± 0.05 mm, a special system similar to the one shown previously in [16] was used to perform the bond. The samples were tested under force control, at a loading rate of $\dot{F}$ by using a uniaxial machine MTS 50kN. The failure stresses are estimated from the average stress [17].

### 2.3. Presentaion of the tubular sample device

The tubular sample is composed of two substrates (7075 T6 aluminum alloy) bonded (Fig. 1(b)) by an adhesive layer as visible in Fig. 1(a). The geometry of the sample is given in Table 1. The height of the substrate is 85.0 mm and the medium radius denoted is 24.75 mm and these are fixed for all the presented configurations. Several FEA model were performed to ensure the stress distribution in the adhesive was not affect.had no effect. Dimensions obtained from this numerical analysis are presented in Table 1.

**Table 1**
Characteristic length of the tubular sample.

| Dimension | Symbol | Value [mm] |
|---|---|---|
| Inner diameter | $\varphi_{ext}$ | 59.0 |
| Outer diameter | $\varphi_{int}$ | 40.0 |
| Mean diameter | $R_m$ | 24.75 |
| Adhesive thickness | $t_a$ | studied parameter |
| Adhesive length | $L_{rc}$ | studied parameter |

Several configurations were tested in this study and are presented in Table 2. The surface prepartion is similiar to the protocol presnetd for Arcan device (maechanical gridding, acetone cleaning and drying) The adjutement ring ensure a similar bonded length between each tested sampels for all configurations in order to provide a good repetability.

#### 2.3.1. Bonding device

The co-axiality of the tubular adherent is guaranteed by the set-up visible in Fig. 1(c) and (d). The position of the first substrate is made by a mechanical stop. After applying adhesive on both sides of the substrate, the second substrate is put in position according to an adjustment ring which determines the bonding length $L_{rc}$. This dimension is then guaranteed to be the same for all the samples by reusing the sample adjustment ring. The sample is clamped onto the bonding set-up as illustrated in Fig. 1(e) during the curing process. A sample was machined in order to cut the substrate along the longitudinal length as seen in Fig. 2(a). The remaining pieces of the adhesive layer (Fig. 2(b)) are observed with an optical microscope Keyence in order to verify the adhesive thickness on the perimeter of the sample. The observed area is delineated by orange square on the Fig. 2b. The values obtained are presented in Fig. 3.

The adhesive thickness is assumed to be constant around the perimeter of the joint (Fig. 3). These results validate the bonding process and set-up.

#### 2.3.2. Testing set-up

The testing device is presented in Fig. 4 the lower clamping device is linked to the sample and the hydraulic cylinder. The upper clamping device is composed of a cardan joint which removes possible bending efforts due to misalignment. The bonded sample is fixed using screws.

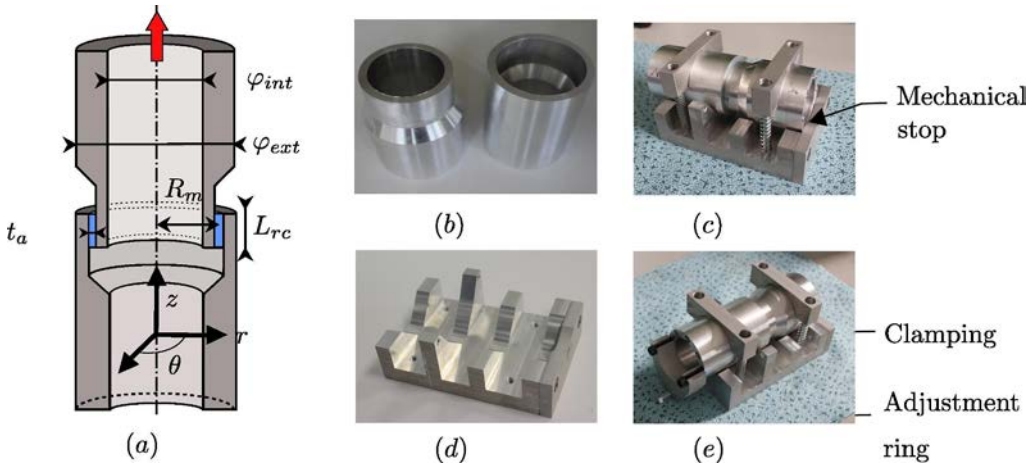


**Fig. 1.** Tubular sample (a) schematic view cut and dimensions (b) aluminum substrates (c) adhesive bonding set-up (d) and (e) clamping and adhesive length control.

**Table 2**
Description of configurations tested.

| Configuration | Adhesive thickness | Bondline length | Loading rate |
|---|---|---|---|
| Configuation 1 | $t_a = 0.2$ | $L_{rc} = 10$ | 0.5 |
| Configuation 2 | $t_a = 0.4$ | $L_{rc} = 10$ | 0.5 |
| Configuation 3 | $t_a = 1.0$ | $L_{rc} = 10$ | 0.5 |
| Configuation 4 | $t_a = 0.4$ | $L_{rc} = 5$ | 0.5 |
| Configuation 5 | $t_a = 0.4$ | $L_{rc} = 20$ | 0.5 |
| Configuation 6 | $t_a = 0.4$ | $L_{rc} = 5$ | 5.0 |

A fully aluminum part was used to guarantee the alignment of the testing device. This part is instrumented with strain gauges and could replace the bonded sample in Fig. 5. The system is considered to be aligned when the four gauges present the same strain values. The alignment is performed using the screws which move the cross of the cardan joint (Fig. 4).

The bonding device is considered to provide good coaxiality of the bonded samples. Then the testing set-up is available to perform tensile testing and reduce the misalignment by using the universal joint (cardan).

## 3. The coupled criterion

The coupled criterion is based on two conditions a stress criterion which describes the onset of micro-cracks in the adhesive layer and an energetic criterion related to the nucleation of these micro-cracks to create a macro-crack as explained in the literature [18,10,19]. Several properties of materials must be identified in order to solve the coupled criterion. The materials' properties and fracture toughness in mode I and II must be identified. Adhesive elastic properties (Young modulus and Poisson's ratio) and strength are identified using a modified Arcan device [20]. Fracture toughness in mode I and II are identified using DCB and ENF test [12,13].

### 3.1. General overview of the failure criteria

According to finite fracture mechanics, crack nucleation is observed in the neighborhood ($\Delta S$) of the free edge of the substrate and the adhesive due to the edge effect. The bonded structure is composed of an adhesive layer denoted $t_a$, and a displacement $d$ is applied as seen in Fig. 6. A reaction force $F_{react}$ is computed numerically from this displacement and will be used to determine the failure load. This point will be discussed in Section 5.2.

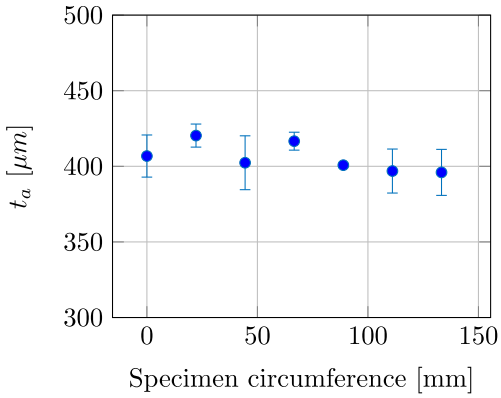


**Fig. 3.** Thickness of the adhesive joint around the tubular sample.

The energetic criterion compares the change in potential energy ($-\Delta W_p/\Delta S$) and the fracture toughness ($G_c$) of the adhesive (Eq. (1)). The fracture toughness presents an evolution according to the mixed-mode as described in [18,?].

$$-\Delta W_p \geqslant G_c.\ \Delta S \tag{1}$$

The potential energy($W_p$) is given by the changes between uncracked ($W_p(0)$) and cracked states ($W_p(S)$) as visible in Eq. (2).

$$-\Delta W_p = W_p(0) - W_p(S) \tag{2}$$

In this paper, the bonded structure is considered under 2D hypothesis. The cracked surface is described by $S = a.\ b$, with $a$ the crack length and $b$ the sample width. The energetic criterion may be written using an incremental energy as expressed by Eq. (3).

$$G^{inc}(a) \geqslant G_c \tag{3}$$

The incremental energy may be delineated by the following expression $G^{inc}(a) = \frac{1}{b}.\ \frac{\Delta S}{a}$. The energetic criterion is fulfilled when the incremental energy exceed $G_c$. The computation of this incremental

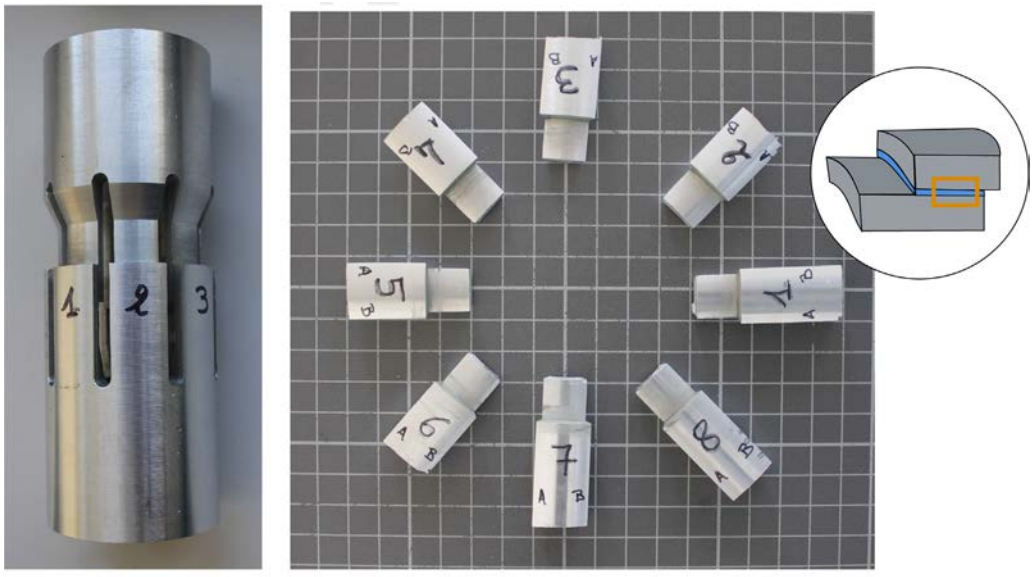


**Fig. 2.** Experimental setup with (a) conventional machine cutting (b) in order to obtain sample around the perimeter.

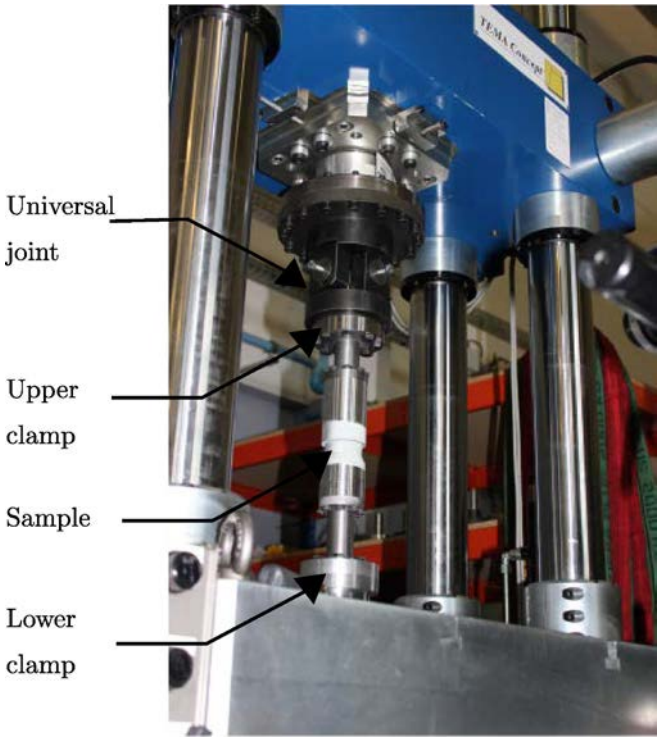


**Fig. 4.** Photograph of the testing devices for tubular samples.

energy based on classical Griffith criterion have been described in a previous paper [21] as presented in Eq. (4).

$$G^{inc}(a) = \frac{1}{a}\int_0^a G(l)dl \tag{4}$$

where $a$ is the cracked length,$l$ is the remaining bonded length ($l = L_{rc} - a$) and $G(l)$ is the energy released rate for the remaining bonded length. The necessity to satisfy simultaneously stress and energetic criteria is explained in [10]. The stress condition assumes that the tensile normal stress reaches the tensile strength. The crack onset may be expressed using the Eq. (5), which implies that the crack onset occurs in the cracked surface defined by the previous criterion.

$$\sigma_{op.}(M) \geqslant Z_N, \forall\, M \in S \tag{5}$$

where $M$ is a point of the expected cracked surface $S$ and fulfils the crack onset conditions given by a stress criterion. The stress for crack

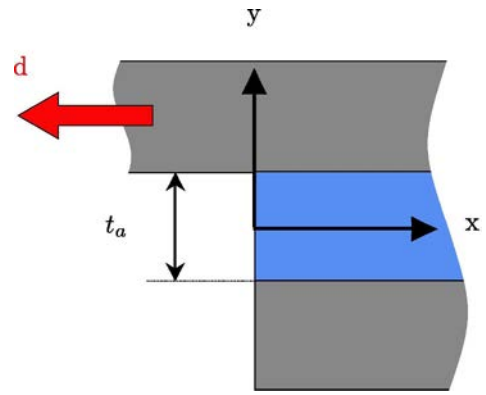


**Fig. 6.** Schematic view of a bonded joint.

onset in opening mode is designated $\sigma_{op.}$ by and the out-of-plane stress (normal to bondline) is designated $Z_N$. By combining Eqs. (3) and (5), the failure of the bonded assembly may be described.

### 3.2. Resolution of the coupled criterion

The incremental energy $G^{inc}$ is presumed to be an increasing function of the crack length as explained in [10]. This first condition leads to a lower limit of the crack length at initiation. The stress $\sigma_{op.}$ is a decreasing function according to the supposed crack length and the stress condition provides the upper limit of the system. The coupled criterion may be solved by combining Eqs. (3) and (5). To solve the system easily, the $G^{inc}$ is assumed to be represented by a dimensionless parameter $A^{inc}(a)$ as described in [18,11]. For single lap joint configuration, some authors indicate a local maximum in the evolution of the incremental energy [18,19,22]. The lower bound related to stress criteria is described by a quadratic criterion, which takes into account out-of-plane and tangential stresses [18]. Similarly to the energetic criterion, the crack onset is turned into a dimensionless parameter $k_{struct}(x)$ [18]. As explained in the literature [18,19,23], the solution of the coupled criterion problem is obtained by using these dimensionless parameters. The parameters $k_{struct}(x) = f(\sigma(x, y), \tau(x, y), Z_N, S_c)$ is a function the stress distribution in the adhesive layer and the failure stress. This parameter is related the stress field in the adhesive bondline. The energetic part is related to the other parameter $A^{inc}(a) = f(G_c(a))$ which depend of the fracture toughness, the dependency to the crack length $a$ is due to the evolution of mode mixity during crack propagation [23,18].

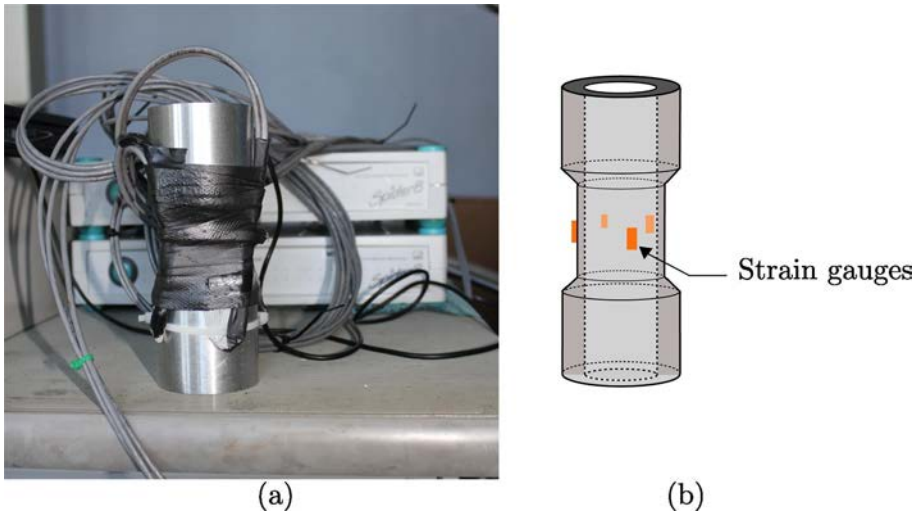


**Fig. 5.** Instrumented sample with strain gauges (a) photograph and (b) schematic view.

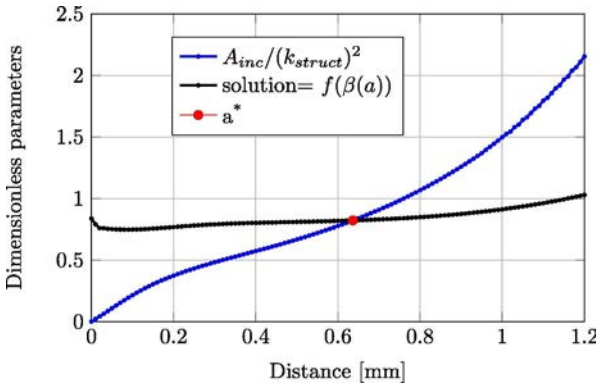


**Fig. 7.** Illustration of the resolution of the coupled criterion.

$$\frac{E^{eq}G_c(a)f(\sigma(x,y),\tau(x,y),Z_N,S_c)}{t_a} = \frac{A^{inc}(a^*)}{[k_{struct}(d^*)]^2} \tag{6}$$

The parameter $E^{eq}$ describes an equivalent modulus of adhesive under 2D assumptions. The energetic criterion (Eq. (4)) and the stress criteria (Eq. (5)) are simultaneously satisfied for a crack length denoted $a^*$ as illustrated in Fig. 7. The solution, is dependent on the mixed-mode denoted $\beta(a)$ [18,23] which is evaluated by Virtual Crack Closure Technique (VCCT) [24,25].

### 3.3. Modification of stress criterion

Previous studies described the crack onset by using a simple stress criterion which considers only the out-of-plane stress [11]. The bi-axial stress state which occurs in the adhesive layer is described by a quadratic criterion by Carrere et al. [26].

$$\sqrt{\left(\frac{\sigma_{yy}(x,y)}{Z_N(\dot{\varepsilon}(x))}\right)^2 + \left(\frac{\tau_{xy}(x,y)}{S_c(\dot{\varepsilon}(x))}\right)^2} \geqslant 1 \tag{7}$$

In the present paper, a quadratic stress criterion is used (Eq. (7)) [18]. Where ($Z_N$) is the out-of-plane strength and ($S_c$) tangential strength. The influence of the strain rate ($\dot{\varepsilon}$) in the adhesive layer as described by Eq. (8) similarly to [17].

$$\begin{cases} Z_N(\dot{\varepsilon}(x)) = \sigma^0_{yy}\left[1+\left(\frac{\dot{\varepsilon}_{yy}}{\dot{\varepsilon}^0_{yy}}\right)^{n_{yy}}\right] \\ S_c(\dot{\varepsilon}(x)) = \tau^0_{xy}\left[1+\left(\frac{\dot{\varepsilon}_{xy}}{\dot{\varepsilon}^0_{xy}}\right)^{n_{xy}}\right] \end{cases} \tag{8}$$

The failure stress according the normal to bondline is $Z_N$ and tangential failure stress is $S_c$. The strain rate for the previous direction is denoted $\dot{\varepsilon}$. In order to describe the influence of strain rate, a reference is taken. Normal stress reference is $\sigma^0_{yy}$ and shear stress reference is $\tau^0_{xy}$. Strain reference for tensile and sher is respectively denoted $\dot{\varepsilon}^0_{yy}$ and $\dot{\varepsilon}^0_{xy}$. The parameters $n_{yy}$ and $n_{xy}$ allow a better description of the failure stress according to the strain rate.

## 4. Experimental results

### 4.1. Identification of adhesive properties

#### 4.1.1. Experimental results of Arcan tests

The identification of the adhesive strength is performed by using the modified Arcan device under traction and shear loading. Three loading rates are used in this study. The failure is symbolized by orange crosses as shown in 8 and ensures repeatability of experimental results.

Fig. 8 shows force–Displacement curves for a loading rate of 0.2kN/s. ND and TD are respectively the normal and tangential displacements. NF and TF are the forces related to the previous displacements. Both curves exhibit brittle behavior of the adhesive. The fracture surface shows a mixed (cohesive/adhesive) failure.

Fig. 9 shows the behavior of the adhesive bonding under a loading rate of 2.0kN/s. The failure force increases with the loading rate as shown by the comparison between Figs. 8 and 9.

Fig. 10 is related to the test under a loading rate of 20kN/s. The force at failure increases with the loading rate. A decrease of ND and TD is also observed.

The normal displacement (ND) is decreasing with the loading rate. For higher loading rate $\dot{F} = 20kN/s$ normalment displacement is in the range of 1 micrometer. The scattered results obtained could be improved by using a more accurate measurement system.

#### 4.1.2. Failure envelope

The failure stress under tension and shear loading is plotted on Fig. 11. The failure envelope is plotted with a dashed line for each loading rate by using Eq. (7).

In order to validate the failure envelope proposed, additional shear-tension loading sample were tested for 0.2 and 2.0 kN/s, five samples were tested for each configuration. The average failure stress obtained is also plotted in Fig. 11. Experimental data and failure envelope (Eq. (8)) are in good agreement for 0.2 and 2.0 kN/s. The fracture surfaces of these samples are visible in Fig. 12.

Eq. (8) describes the relationship between failure stress and strain rate. The strain rate is computed from the force–displacement curve as detailed in [17]. Fig. 13 presents the evolution of assembly strength according to the strain rate under tension and shear loading.

Based on the experimental data, the identified parameters are listed in Table 3. The identification of the parameters is performed using a Least Square minimization method (library lmfit in Python). The proposed law is visible in Fig. 13 and is presented by a dashed line.

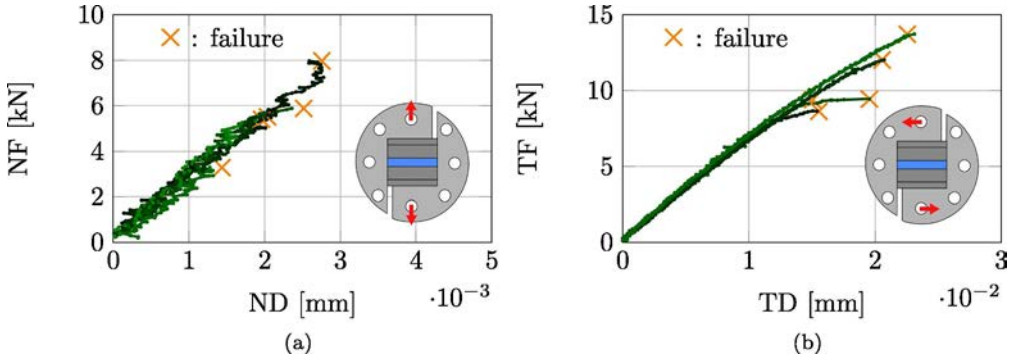


**Fig. 8.** Force displacement curves of Arcan samples tested at a loading rate of 0.2 kN/s (a) under tension (Normal Force: NF versus Normal Displacement: ND) and (b) shear loading (Tangential Force: TF versus Tangential Displacement: TD).

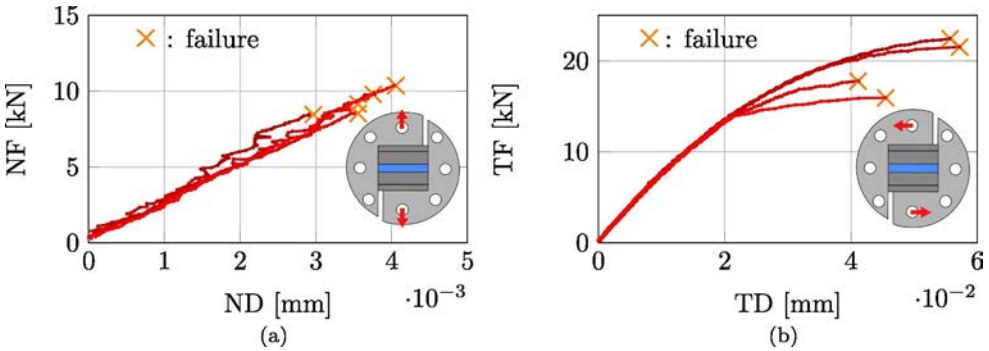


**Fig. 9.** Force displacement curves of Arcan samples tested at a loading rate of 2.0 kN/s (a) under tension (Normal Force: NF versus Normal Displacement: ND) and (b) shear loading (Tangential Force: TF versus Tangential Displacement: TD).

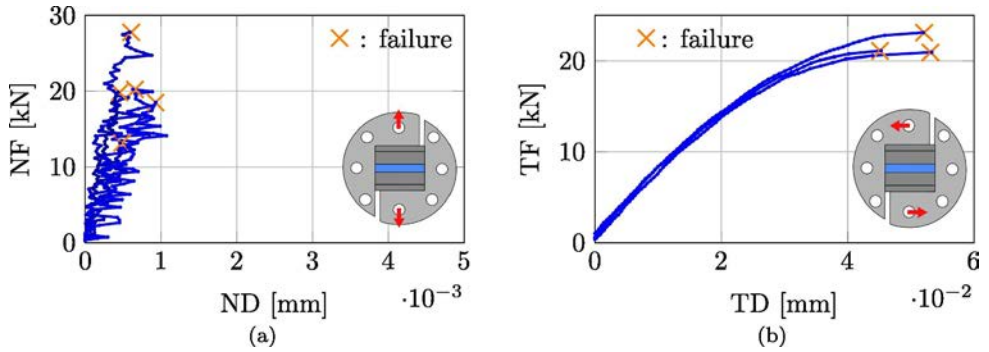


**Fig. 10.** Force displacement curves of Arcan samples tested at a loading rate of 20.0 kN/s (a) under tension (Normal Force: NF versus Normal Displacement: ND) and (b) shear loading (Tangential Force: TF versus Tangential Displacement: TD).

### *4.2. Validation on tubular sample*

The previous section detailed the identification procedure of the elastic parameter and the fracture strength. In order to validate the dimensioning approach, tubular bonded samples were also tested. Several parameters were investigated, the adhesive overlap length ($L_{rc}$), the adhesive thickness ($t_a$) and the influence of the loading rate ($\dot{F}$).

#### *4.2.1. Influence of bondline length*

Fig. 14(a) shows the force–displacement curves for an overlap length of 5 mm and an adhesive thickness of 0.4 mm. Five samples were tested at a loading rate of 0.5 kN/s. The assembly presents a brittle behavior. The fracture surfaces obtained were mixed as shown in Fig. 14(b).

The failure load increases with bonded length as shown in Fig. 15. The linear behaviour of the adhesive is visible, yet the failure load is relatively scattered (see Fig. 16).

As noticed for bonded of $L_{rc}$ = 5 mm and 10 mm, the failure load increased with a bonded length of 20 mm.

Except for failure, the force displacement curves shows a good repeatability of the bonded sample tested. The failure load increases with the bonded length. The fracture surfaces present are all a mix of cohesive and adhesive which could explain the scattered results obtained.

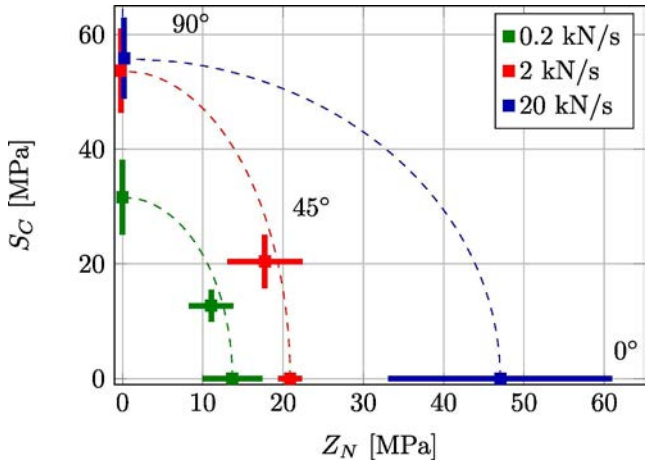


**Fig. 11.** Failure envelope of the adhesive bonding for three loading rates.

#### *4.2.2. Influence of adhesive thickness*

Experimental tests were performed to estimate the influence of bondline thickness on the failure load. As visible in Fig. 17, the non-linear section of the curve is larger than before the failure of the sample as seen in Fig. 15.

The increasing in bondline thickness results in a decrease in the failure load as shown in Fig. 18. The observation of the fracture surface reveals the presence of air bubbles as seen in Fig. 18(b).

The failure decrease with the bondline thickness. Some defects are visible on post-mortem fracture surfaces for $t_a$ = 1.0 mm.

#### *4.2.3. Influence of loading rate*

A final experimental campaign was performed, two loading rates were tested: $\dot{F}$ = 0.5 kN/s and 5.0 kN/s and estimate the influence on

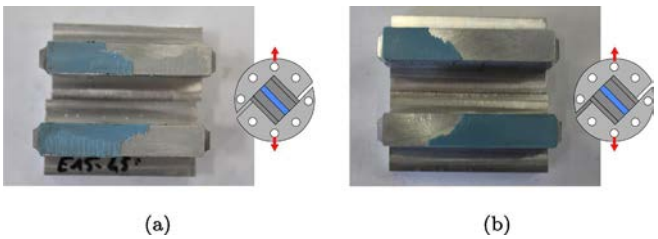


**Fig. 12.** Fracture surfaces on Arcan samples tested under shear-tension loading at a loading rate of (a) 0.2 kN/s and (b) 2.0 kN/s.

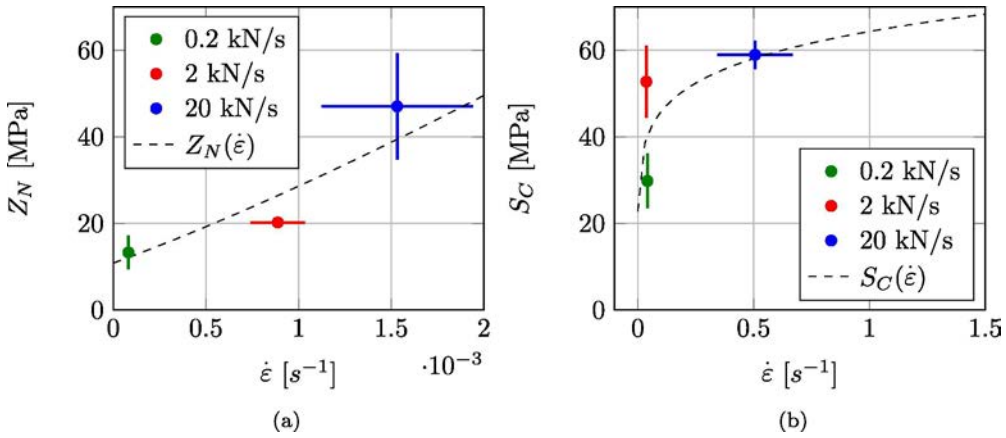


**Fig. 13.** Evolution of the ultimate stress according to the speed loading under (a) tension and (b) shear loading.

**Table 3**
Parameters identified for the stress dependent on the strain rate.

| Symbol | Value |
|---|---|
| $\sigma^0_{yy}$ | 15.77 [MPa] |
| $\tau^0_{xy}$ | 22.745 [MPa] |
| $n_{yy}$ | 0.531 |
| $n_{xy}$ | 0.175 |
| $\varepsilon^0_{yy} = \varepsilon^0_{xy}$ | $9.10^{-4}$ [$s^{-1}$] |

the failure load. The results obtained for $\dot{F} = 0.5$ kN.s are shown in Fig. 19. The comparative analysis of Fig. 14(a) and Fig. 19 shows an increase in the failure load proportional to the loading rate. No significant changes were present on the fracture surfaces.

## 5. Numerical failure load prediction

In order to assess the modification proposed on the coupled criterion, a comparison between experimental work and numerical models is performed. The application of the coupled criterion to the tubular sample is described in the next section.

### 5.1. Model

An axisymmetric model was performed to represent the tubular sample as shown in Fig. 20. Each end of the substrate is linked to a reference point (RP), a displacement is applied on the upper $RP_H$ and the lower $RP_B$ is clamped. In the case shown, the applied displacement is $d = 1.0$ mm.

A refined mesh with a characteristic length of $10^{-2}$ mm is used in the region of the adhesive layer as shown in Fig. 20. For the present model ($L_{rc} = 5.0$ mm, $t_a = 0.4$ mm), 723 368 elements CGAX4R and CGAX3 in Abaqus Standard were used. Carrere et al. [18] recommend 40 elements in the adhesive thickness of single lap joint geometry to obtain the convergence of the failure load applied. Based on previous study [14], 40 elements in the joint thickness gives satisfying results. According to these work, the mesh size is considered fine enough to obtain reliable failure load prediction. Stress and strain discussed in the following section are considered at the position $r = R_m - \frac{t_a}{2}$. The position corresponds to the internal interface between the adhesive layer and the internal substrate. The maximum stress concentration was located on this line according to the FEA results.

### 5.2. Coupled criterion application

As explained previously, a displacement is applied on the upper reference point. The reaction force ($F_{react}$) due to the displacement is computed. The duration of the test ($\Delta t_{test}$) may be estimated according to Eq. (9).

$$\Delta t_{test} = \frac{F_{react}}{\dot{F}} \tag{9}$$

where $\dot{F}$, is the loading rate of tested samples. Strain distribution along the joint length at $r = R_m - \frac{t_a}{2}$ is considered. Under elastic assumption, the strain rate may be estimated using Eq. (10). The present methodology is applied to a brittle adhevive joint (Figs. 9 and 10). For adhesive bonding exhibiting strong non linear behavior, the present methodology will present limitations. Out-of-plane and tangential strain distributions are given in Fig. 21(a) for the tubular sample ($L_{rc} = 5.0$ mm, $t_a = 0.4$ mm).

$$\dot{\varepsilon} = \frac{\varepsilon}{\Delta t_{test}} \tag{10}$$

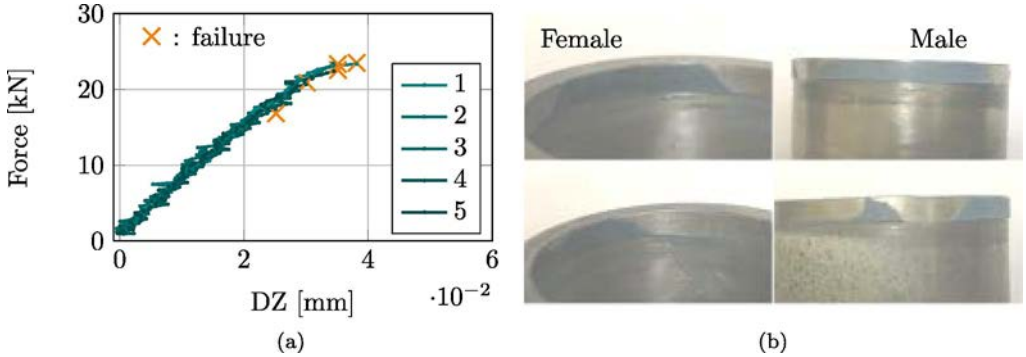


**Fig. 14.** Tubular sample Lrc = 5 mm and ta = 0.4 mm: (a) Force–displacement curve performed at a loading rate of 0.5 kN/s and (b) fracture surface.

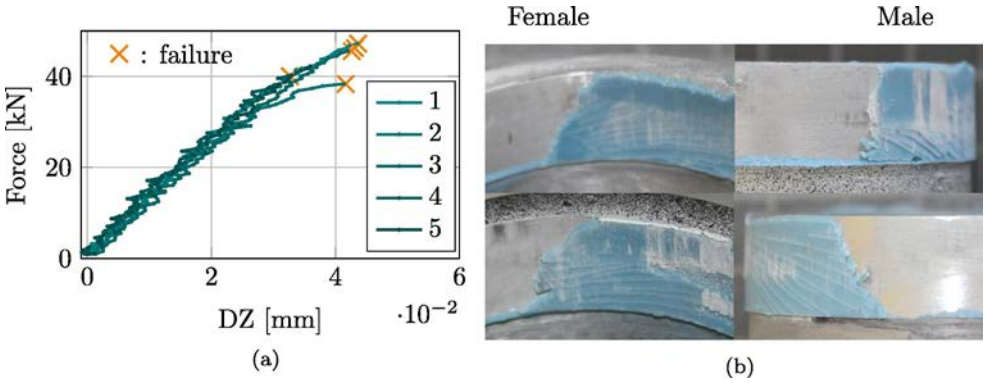


**Fig. 15.** Tubular sample Lrc = 10 mm and ta = 0.4 mm: (a) Force–displacement curve performed at a loading rate of 0.5 kN/s and (b) fracture surface.

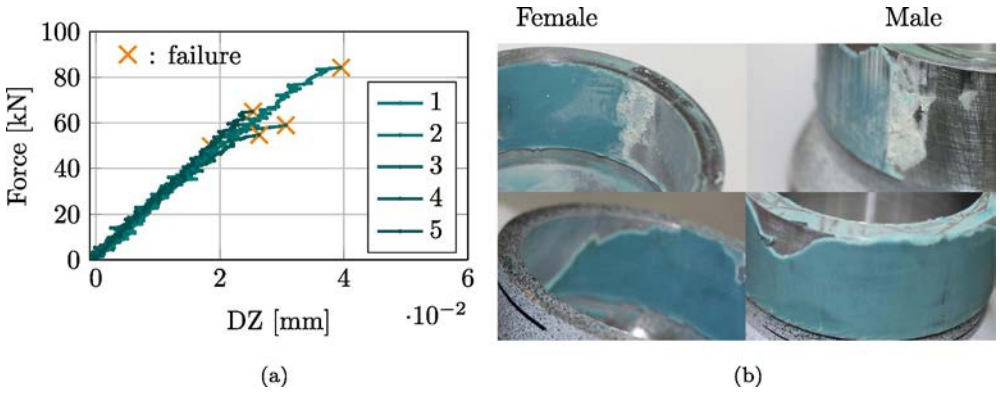


**Fig. 16.** Tubular sample Lrc = 20 mm and ta = 0.4 mm: (a) Force–displacement curve performed at a loading rate of 0.5 kN/s and (b) fracture surface.

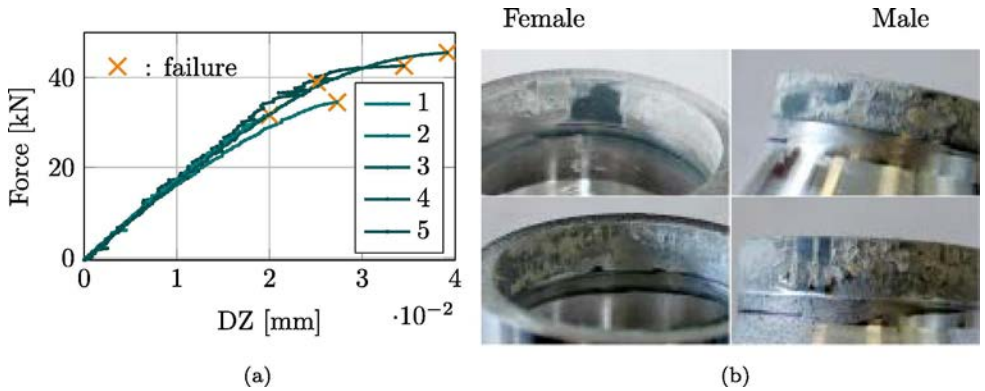


**Fig. 17.** Tubular sample Lrc = 10 mm and ta = 0.2 m: (a) Force–displacement curve performed at a loading rate of 0.5 kN/s and (b) fracture surface.

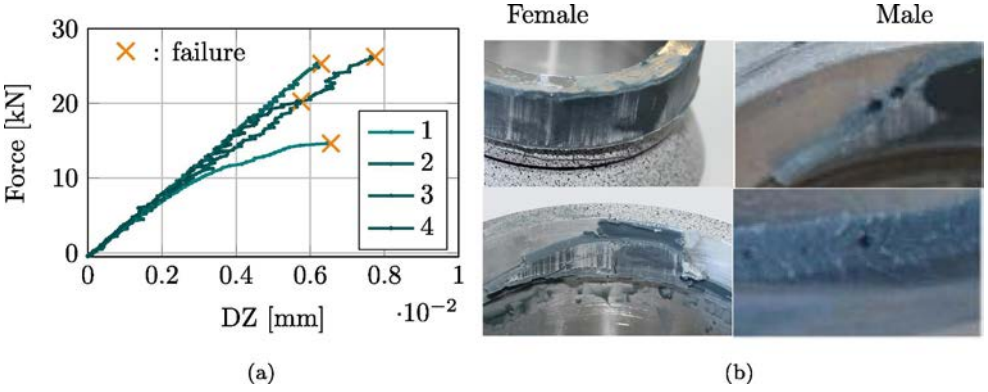


**Fig. 18.** Tubular sample Lrc = 10 mm and ta = 1.0 m: (a) Force–displacement curve performed at a loading rate of 0.5 kN/s and (b) fracture surface.

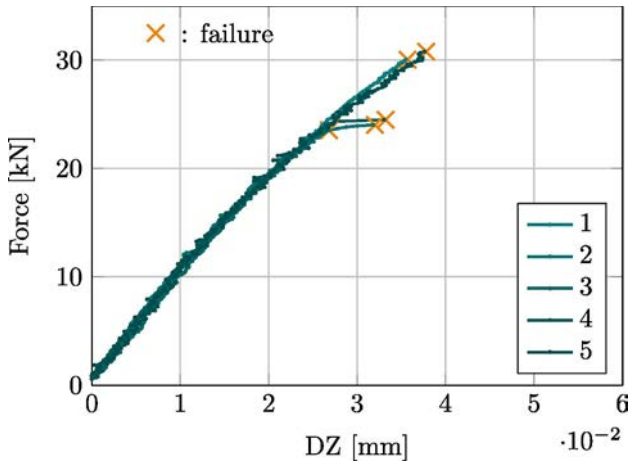


**Fig. 19.** Tubular sample Lrc = 5 mm and ta = 0.4 m: Force–displacement curve performed at a loading rate of 5.0 kN/s and.

The computed strain near to the edge is strongly affect by singular stress field. The resolution of the coupled criterion is performed at a distance denoted $a^*$ from the free edge. This assumption free the failure load prediction from singular stress field. The strain $\varepsilon$ is calculated by FEM analysis and is presented on Fig. 21(a). Then, the strain rate $\dot{\varepsilon}$ along the overlap length is calculated by using Eq. (10). By using Eq. (8) the adhesive strength is calculated and is shown on Fig. 21(b). This stress state is obtained under elastic assumption for an applied displacement $d$ (Fig. 20).

Section 3 briefly describes both energetic and stress based criteria. In order to solve the coupled criterion easily, dimensionless parameters are used as detailed in [18,11]. $k_{struct}(x)$ represents the evolution of the stress state in the adhesive layer, under 2D assumption and considering a bi-axial loading. Fig. 22 shows the evolution of this parameter along the interface ($r = R_m - \frac{t_a}{2}$ Fig. 20). This parameter represents the stress criterion and decreases steadily according to the distance from the free edges. The coupled criterion will be solved at a specific distance from the free edge by using Eq. (6).

The energetic criterion given in Eq. (3) compares the incremental energy $G^{inc}$. and the critical energy release rate $G_c$. Mesh unbuttoning is performed similarly to [18] to simulate the crack propagation. In order to easily solve the coupled criterion, $A^{inc}(a)$ is used as a dimensionless parameter which is dependent on the crack length because of the mixed mode. VCCT is performed to estimate the evolution of the mixed mode. As shown in Fig. 23, the dimensionless parameter exhibits a local maximum followed by a local minimum, then an increasing curve. In the area

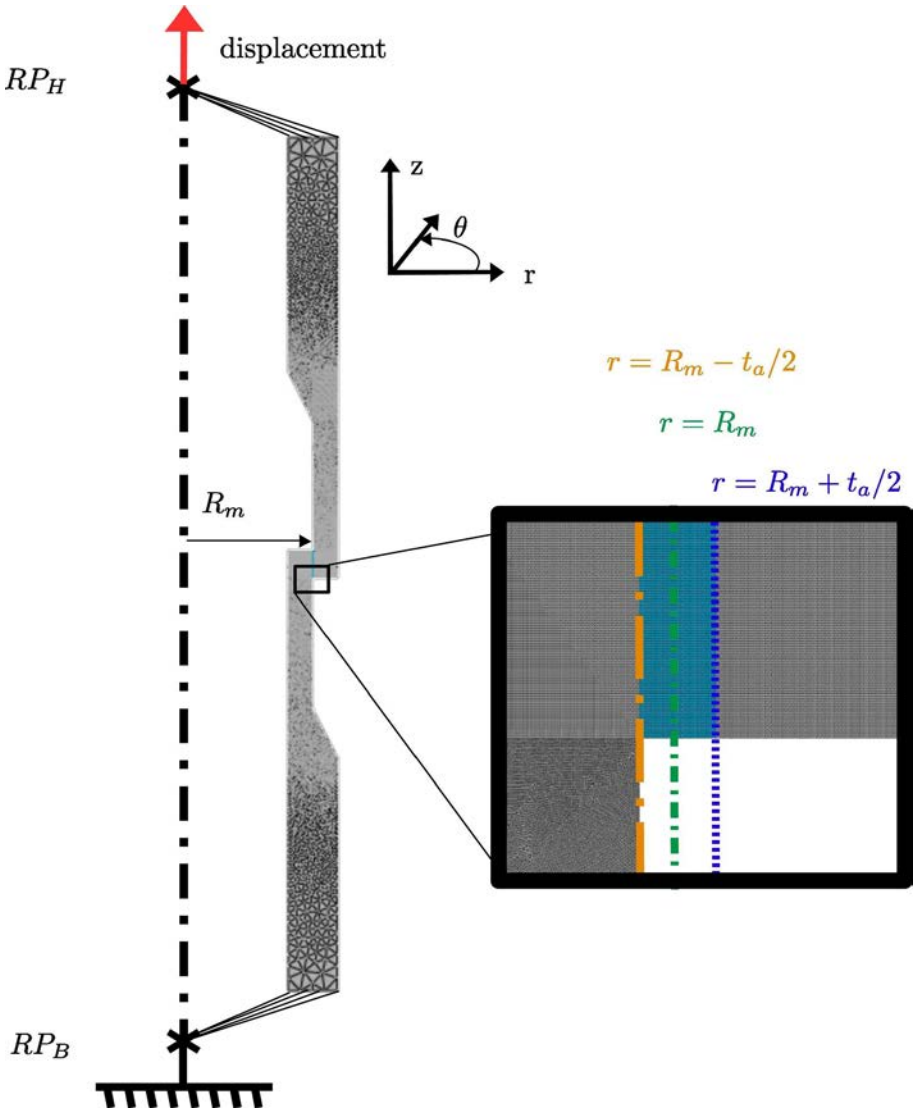


**Fig. 20.** Schematic view of a bonded joint.

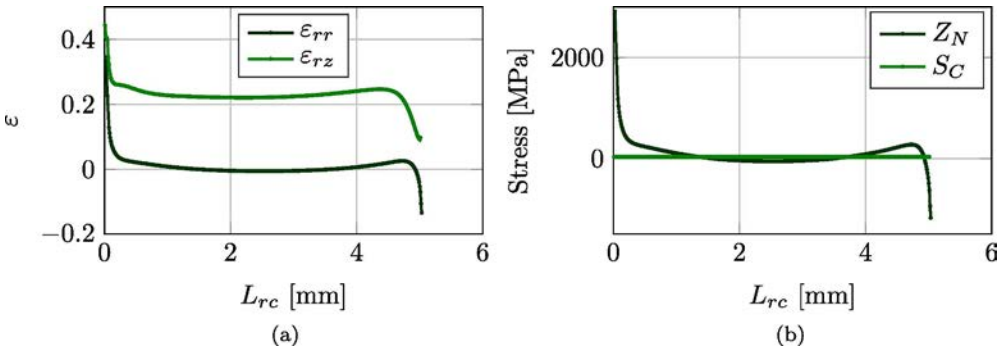


**Fig. 21.** Tubular sample Lrc = 5 mm and ta = 0.4 mm: (a) strain evolution along the adhesive length at the interface and (b) ultimate stress calculated.

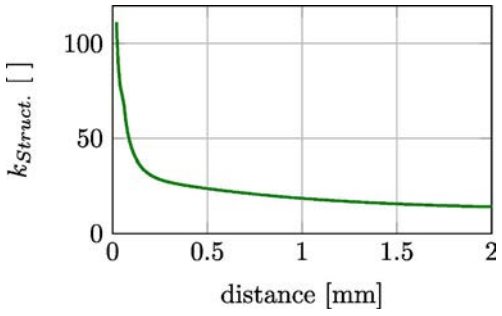


**Fig. 22.** Evolution the dimensionless parameter $k_{struct}(x)$ along the interface $r = R_m - \frac{t_a}{2}$ for a tubular sample.

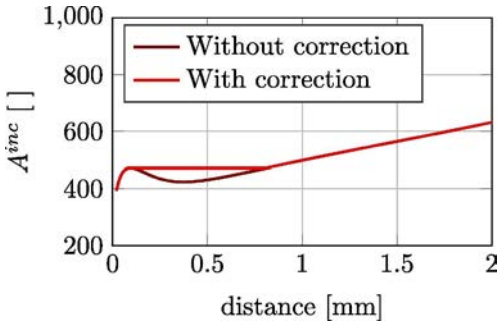


**Fig. 23.** Evolution the dimensionless parameter $A^{inc}(a)$ for a crack propagation along the interface $r = R_m - \frac{t_a}{2}$ for a tubular sample.

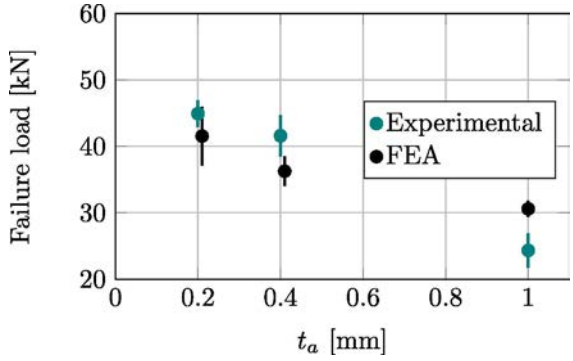


**Fig. 24.** Comparison of the failure load prediction and experimental data for three adhesive thicknesses.

of the local minimum, the energetic parameter is assumed to be constant. This correction was applied for single lap joint geometries in [18,22].

The resolution of the coupled criterion is performed using dimensionless parameters (Eq. (6)). Both energetic and stress-based criteria are simultaneously satisfied for an internal length denoted $a^*$. The resolution procedure is detailed in the literature in [18].

## 6. Discussion

The failure strength properties of the adhesive were identified by performing Arcan tests as described in Section 4.1.2. The fracture toughness of the adhesive in mode I and II comes from the literature [13,12]. The failure predictions of the tubular bonding are performed according to the procedure described in Sections 2.3.1 and 2.3.2. The influence of the adhesive thickness obtained experimentally is shown in Fig. 24. Because of the non uniform stress distribution in the bonded joint, the failure load is presented in kN. The computation of an equivalent stress seems difficult. For lower adhesive thickness ($t_a$ 0.2 and 0.4 mm), the comparison between experimental data and failure prediction obtained by coupled criterion is in good agreement. The failure predictions are conservative for the previous adhesive thickness at a loading rate of 0.5kN/s. However, for 1.0 mm thick joint, the numerical failure prediction is higher than the experimental data. Observation of the fracture surface (Fig. 18(b)) shows porosity with large diameter air bubbles. However, the numerical simulation takes into account a model without any defects. These points could explain the non-conservative prediction for higher adhesive thickness.

A second experimental campaign was performed to analyse the effect of the overlap length as shown in Fig. 25. The failure predictions obtained by FEA are in good agreement with experimental data.

The last experimental campaign deals with the influence of the loading rate on the failure load of the bonded assembly. Tubular samples with an overlap length of 5 mm and adhesive thickness of 0.4 mm were tested at 0.5 and 5.0 kN/s as presented in Fig. 26. The failure load increases with the loading rate.

The modification of the stress-based criterion accounts for the evolution of the failure load according to the loading rate. However, the numerical results are still conservative compared to experimental data.

## 7. Conclusions

In this paper, the numerical estimation of the failure of bonded joints was obtained by using a coupled criterion. The failure of the bonded joints is considered to occur when both stress based and energetic based criteria are satisfied simultaneously at a certain distance from the singular point. This criterion is performed by using material strength and fracture toughness of the adhesive. In order to take into account the loading rate effect on the failure load of the bonded structure, a modification of the stress criterion was proposed in this paper. The adhesive strength was estimated with a modified Arcan test at three loading rates. A tubular bonded sample was designed in order to evaluate the validity of the proposed approach. Both the bonded set-up and the loading device were carefully investigated to guarantee the obtained results. Then, a comparison between experimental and numerical failure load was performed. The proposed method presents a good agreement between numerical and experimental for different

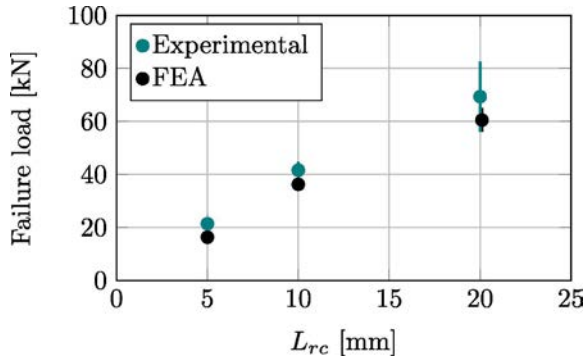


**Fig. 25.** Comparison of the failure load prediction and experimental data for three adhesive overlap lengths.

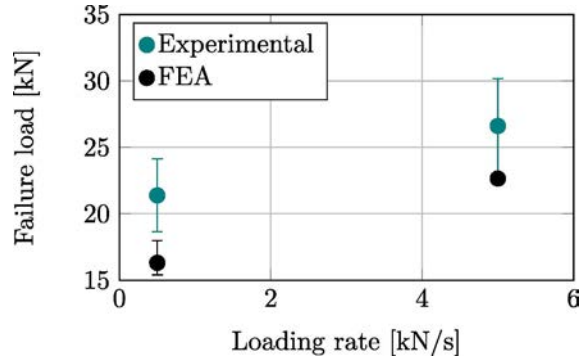


**Fig. 26.** Tubular sample $L_{rc} = 5$ mm and $t_a = 0.4$ mm: comparison of the failure load prediction and experimental data for two loading rates.

configurations (bondline length and thickness). The modification of the stress based criterion is able predict the evolution of the loading rate. As a first perspective on the current work, the behavior of a bonded joint under complex loading could be investigated with the tubular sample (torsion, tensile torsion combined or separated). In addition to that, other modifications of the coupled criterion must be implemented to take into account the non-linear behaviour of the adhesive materials. Finally, the fatigue behaviour of bonded joints could be investigated by using the tubular sample. The influence of cyclic and alternate loading could be performed using the proposed tubular devices.

## Declaration of Competing Interest

The authors declare that they have no known competing financial interests or personal relationships that could have appeared to influence the work reported in this paper.

## Acknowledgements

The authors would like to thank the CNES and ArianeGroup for the support provided within the framework of an R&T CNES project.

## References

[1] D.B. Bogy, K.C. Wang, Stress singularities at interface corners in bonded dissimilar isotropic elastic materials, Int. J. Solids Struct. 7 (8) (1971) 993–1005, https://doi.org/10.1016/0020-7683(71)90077-1.

[2] Y. Zhang, P. Wu, M. Duan, A mesh-independent technique to evaluate stress singularities in adhesive joints, Int. J. Adhes. Adhes. 57 (2015) 105–117, https://doi.org/10.1016/j.ijadhadh.2014.12.003.

[3] N.-A. Noda, R. Li, T. Miyazaki, R. Takaki, Y. Sano, Convenient adhesive strength evaluation method in terms of the intensity of singular stress field $\lambda\theta\beta$. https://doi.org/10.1142/S0219876218500858.

[4] N.-a. Noda, F. Ren, R. Takaki, Z. Wang, K. Oda, T. Miyazaki, Intensity of singular stress field over the entire bond line thickness range useful for evaluating the adhesive strength for plate and cylinder butt joints, Int. J. Adhes. Adhes. 85 (June) (2018) 234–250. https://doi.org/10.1016/j.ijadhadh.2018.05.013.

[5] R. Li, N.-a. Noda, R. Takaki, Y. Sano, Y. Takase, T. Miyazaki, Most suitable evaluation method for adhesive strength to minimize bend effect in lap joints in terms of the intensity of singular stress field 86 (August) (2018) 45–58. doi:10.1016/j.ijadhadh.2018.08.006.

[6] L. Goglio, M. Rossetto, E. Dragoni, Design of adhesive joints based on peak elastic stresses, Int. J. Adhes. Adhes. 28 (8) (2008) 427–435, https://doi.org/10.1016/j.ijadhadh.2008.04.001.

[7] E. Dragoni, L. Goglio, F. Kleiner, Designing bonded joints by means of the JointCalc software, Int. J. Adhes. Adhes. 30 (5) (2010) 267–280, https://doi.org/10.1016/j.ijadhadh.2009.11.002.

[8] J. Whitney, R. Nuismer, Stress fracture criteria for laminated composites containing stress concentrations, J. Compos. Mater. 8) (July 2974) (1974) 253–265.

[9] H.A. Whitworth, O. Aluko, N.A. Tomlinson, Application of the point stress criterion to the failure of composite pinned joints, Eng. Fract. Mech. 75 (75) (2008) 1829–1839, https://doi.org/10.1016/j.engfracmech.2006.12.003.

[10] D. Leguillon, Strength or toughness? A criterion for crack onset at a notch, Eur. J. Mech., A/Solids 21 (1) (2002) 61–72, https://doi.org/10.1016/S0997-7538(01)01184-6.

[11] A. Moradi, N. Carrère, D. Leguillon, E. Martin, J.Y. Cognard, Strength prediction of bonded assemblies using a coupled criterion under elastic assumptions: effect of material and geometrical parameters, Int. J. Adhes. Adhes. 47 (2013) 73–82, https://doi.org/10.1016/j.ijadhadh.2013.09.044.

[12] N.B. Salem, M.K. Budzik, J. Jumel, M.E.R. Shanahan, F. Lavelle, Investigation of the crack front process zone in the Double Cantilever Beam test with backface strain monitoring technique, Eng. Fract. Mech. 98 (2013) 272–283, https://doi.org/10.1016/j.engfracmech.2012.09.028.

[13] J. Jumel, M.K. Budzik, N. Ben Salem, M.E.R. Shanahan, Instrumented end notched flexure - Crack propagation and process zone monitoring. Part I: modelling and analysis, Int. J. Solids Struct. 50 (2) (2013) 297–309, https://doi.org/10.1016/j.ijsolstr.2012.08.030.

[14] J. Le Pavic, G. Stamoulis, T. Bonnemains, D. Da Silva, D. Thévenet, Fast failure prediction of adhesively bonded structures using a coupled stress-energetic failure criterion, Fatigue Fract. Eng. Mater. Struct. (May) (2018) 1–13, https://doi.org/10.1111/ffe.12938.

[15] N. Arnaud, R. Créac'Hcadec, J.Y. Cognard, A tension/compression-torsion test suited to analyze the mechanical behaviour of adhesives under non-proportional loadings, Int. J. Adhes. Adhes. 53 (2014) 3–14, https://doi.org/10.1016/j.ijadhadh.2014.01.013.

[16] A. Ilioni, C. Badulescu, N. Carrère, P. Davies, D. Thévenet, A viscoelastic-visco-plastic model to describe creep and strain rate effects on the mechanical behaviour of adhesively-bonded assemblies, Int. J. Adhes. Adhes. https://doi.org/10.1016/j.ijadhadh.2017.12.003.

[17] L. Dufour, B. Bourel, F. Lauro, G. Haugou, N. Leconte, N. Carrere, Failure stress criterion for adhesively bonded joint at different strain rates by using dynamic Arcan test device, EPJWeb of Conferences 01024 (94). https://doi.org/10.1051/epjconf/20159401024.

[18] N. Carrere, E. Martin, D. Leguillon, Comparison between models based on a coupled criterion for the prediction of the failure of adhesively bonded joints, Eng. Fract. Mech. 138 (2015) 185–201, https://doi.org/10.1016/j.engfracmech.2015.03.004.

[19] A. Moradi, D. Leguillon, N. Carrère, Influence of the adhesive thickness on a debonding - an asymptotic model, Eng. Fract. Mech. 114 (2013) 55–68, https://doi.org/10.1016/j.engfracmech.2013.10.008.

[20] J.Y. Cognard, R. Créac'hcadec, L. Sohier, P. Davies, Analysis of the nonlinear behavior of adhesives in bonded assemblies-Comparison of TAST and Arcan tests, Int. J. Adhes. Adhes. 28 (8) (2008) 393–404, https://doi.org/10.1016/j.ijadhadh.2008.04.006.

[21] E. Martin, D. Leguillon, Energetic conditions for interfacial failure in the vicinity of a matrix crack in brittle matrix composites 41 (2004) 6937–6948. https://doi.org/10.1016/j.ijsolstr.2004.05.044.

[22] S. Hell, P. Weißgraeber, J. Felger, W. Becker, A coupled stress and energy criterion for the assessment of crack initiation in single lap joints: a numerical approach, Eng. Fract. Mech. 117 (2014) 112–126, https://doi.org/10.1016/j.engfracmech.2014.01.012 http://www.sciencedirect.com/science/article/pii/S0013794414000228.

[23] E. Martin, T. Vandellos, D. Leguillon, N. Carrère, Initiation of edge debonding: coupled criterion versus cohesive zone model (2016) 157–168. doi:10.1007/s10704-016-0101-2.

[24] E.F. Rybicki, M.F. Kanninen, A finite element calculation of stress intensity factors by a modified crack closure integral, Eng. Fract. Mech. 9 (1) (1977) 931–938.

[25] T.K. O'Brien, Characterization of delamination onset and growth in a composite laminate, Damage Compos. Mater. ASTM STP 7 (1982) 140–167.

[26] N. Carrere, C. Badulescu, J. Cognard, D. Leguillon, 3D models of specimens with a scarf joint to test the adhesive and cohesive multi-axial behavior of adhesives, Int. J. Adhes. Adhes. 62 (2015) 154–164, https://doi.org/10.1016/j.ijadhadh.2015.07.005.